

NUMERICAL MLPG ANALYSIS OF PIEZOELECTRIC SENSOR IN STRUCTURES

Peter STAŇÁK^{1*}, Ján SLÁDEK¹, Vladimír SLÁDEK¹, Slavomír KRAHULEC¹

Abstract

The paper deals with a numerical analysis of the electro-mechanical response of piezoelectric sensors subjected to an external non-uniform displacement field. The meshless method based on the local Petrov-Galerkin (MLPG) approach is utilized for the numerical solution of a boundary value problem for the coupled electro-mechanical fields that characterize the piezoelectric material. The sensor is modeled as a 3-D piezoelectric solid. The transient effects are not considered. Using the present MLPG approach, the assumed solid of the cylindrical shape is discretized with nodal points only, and a small spherical subdomain is introduced around each nodal point. Local integral equations constructed from the weak form of governing PDEs are defined over these local subdomains. A moving least-squares (MLS) approximation scheme is used to approximate the spatial variations of the unknown field variables, and the Heaviside unit step function is used as a test function. The electric field induced on the sensor is studied in a numerical example for two loading scenarios.

Address

¹ Institute of Construction and Architecture, Slovak Academy of Sciences, Dúbravská cesta 9, 845 03 Bratislava, Slovakia

* **Corresponding author:** usarpsta@savba.sk

Key words

- Meshless Local Petrov-Galerkin (MLPG) method,
- MLS approximation,
- piezoelectric solids,
- induced electric field.

1 INTRODUCTION

A broad range of engineering applications, smart structures and devices take advantage of piezoelectric materials. Piezoelectric materials are often referred to as smart materials. The coupling between the mechanical and electric behavior in piezoelectric material allows for the transformation of the mechanical energy to electrical energy and vice-versa; thus such material operates as an energy transducer. They are extensively utilized as ultrasound devices, sensors and actuators in many engineering and industrial fields including aeronautics, space, defense, railways and sports equipment. A great deal of research in civil engineering has been conducted on designing active types of damping systems for flexible multi-story structures in order to reduce the dynamic response due to external excitations such as earthquakes and wind (Adachi et al., 2004; Fur, et al., 1996). Active damping using piezoelectric actuators achieves an excellent vibration suppression performance; however, it requires a large amount of an

external power supply (Agnes, 1995; Ahmadian and DeGiulio, 2001). Sensors must be attached to the host structure together with the actuators in order to respond to any external stimulus. Applications for structural health monitoring (SHM) and deflection sensing are gaining increased attention (Song et al., 2006). New applications are still emerging that are accompanied with a significant research interest in the field of numerical modelling and applied mechanics.

The solution of boundary value problems for structures with piezoelectric components requires advanced numerical methods due to the above-mentioned coupling of mechanical and electrical fields occurring in piezoelectric materials. The numerical analysis of piezoelectric devices has been dominated by mesh-based methods such as the finite element method (FEM) and the boundary element method (BEM). Analytical solutions such as (Heyliger, 1997; Ray et al., 1998) are limited to simple geometries and boundary conditions. FEM is widely used in the design of structures (Benjeddou, 2000; Lerch, 1990) incorporating piezoelectric materials; however, it

possesses some drawbacks, e.g. shear-locking of elements during the modeling of thin-walled structures, which is eliminated only at a high computational cost and lower degree of accuracy. BEM has been applied to the analysis of piezoelectric materials (Ding and Liang, 1999; Lee, 1995); however, it is limited by the unavailability of fundamental solutions for 3-D problems in piezoelectric anisotropic materials.

Meshless methods for the solution of various boundary value problems are powerful alternatives to mesh-based techniques. Meshless methods are also characterized by high adaptivity and a low cost to prepare the input and output data for numerical analyses. Many drawbacks of mesh-based methods can be efficiently eliminated if only nodal points are used instead of finite elements. The meshless Local Petrov-Galerkin (MLPG) method (Atluri and Zhu, 1998; Atluri, 2004) is considered to be one of the most popular meshless methods. The MLPG has been successfully applied to various problems related to piezoelectricity, including 2-D problems (Sladek, et al., 2006), thermopiezoelectricity (Sladek et al., 2010a) and piezoelectric rectangular and laminated plates (Sladek et al., 2010b; Sladek et al., 2012b). An investigation of magnetolectric effects in composites with piezoelectric and piezomagnetic layers has been recently conducted by Sladek et al. (2012a). The advantages of meshless formulations for the fracture analysis of piezoelectric solids have been shown in (Sladek et al., 2007). As a special case of 3-D problems, axisymmetric solids were analysed (Sladek et al., 2008) as well as axisymmetric circular plates (Sladek et al., 2012c; Stanak et al., 2011). The axial symmetry of the assumed geometry reduces the original 3-D problem to a 2-D problem in the angular cross section.

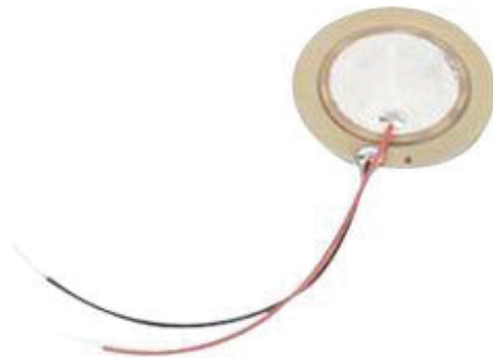


Fig. 1 Typical piezoelectric device used as a deformation sensor.

The majority of piezoelectric sensors used for sound resonators or deformation sensors have a cylindrical shape as shown in Fig. 1. These devices may be used in civil engineering applications such as intelligent houses for the operation of floor-switching air-conditioning, smart lighting systems or burglar detection. If a sensor is loaded in bending, it may be convenient to analyze it numerically as a piezoelectric circular plate (Sladek et al., 2012c). On the other hand, if the sensor is loaded in compression with a non-uniform load distribution, a numerical model for a general 3-D piezoelectric solid body is required. The present paper thus gives an extension of the MLPG method to 3-D piezoelectric solids, since previous works only included 3-D elastic solids (Sladek et al., 2009). Uniform and non-uniform load distributions at the top of the body are considered. The mechanical displacement applied corresponds to an idealized case when the sensor is a part of a deformed composite panel. Three loading scenarios are considered, depending on the position and orientation of the prescribed load.

The coupled electro-mechanical fields for piezoelectric material are described by constitutive relations and governing partial differential equations (PDEs). Nodal points are spread on the analyzed do-

main without any limitations on their mutual positions. A small local subdomain of a spherical shape is introduced around each nodal point. Local integral equations (LIEs) constructed from the governing PDEs are defined over these spherical subdomains. A Heaviside unit step function is applied as a test function in each local subdomain, which leads to a pure boundary integral formulation. The LIEs obtained are non-singular and possess a very simple form. If a simple shape like a sphere is chosen for the geometry of the local subdomains, numerical integrations can be easily carried out over them. The Moving Least-Squares (MLS) approximation scheme (Atluri, 2004; Lancaster and Salkauskas, 1981) is used to approximate the spatial variations of all the physical fields in terms of the specific nodal values. The essential boundary conditions at the global boundary are specified by the collocation of the MLS approximations for the prescribed field quantities at the boundary nodes. Numerical examples are presented for the piezoelectric body of a cylindrical shape to assess the applicability of the proposed MLPG method.

2 GOVERNING EQUATIONS FOR COUPLED ELECTRO-MECHANICAL FIELDS

The constitutive equations of piezoelectric material represent a coupling of the mechanical and electrical fields. The influence of the temperature is ignored, so the pyroelectric effect is not considered. The piezoelectric constitutive equations given by Tiersten (1969) are expressed as converse and direct linear piezoelectric equations, respectively

$$\sigma_{ij}(\mathbf{x}) = C_{ijkl} \varepsilon_{kl}(\mathbf{x}) - e_{kij} E_k(\mathbf{x}) \quad (1)$$

$$D_i(\mathbf{x}) = e_{ikl} \varepsilon_{kl}(\mathbf{x}) + h_{ik} E_k(\mathbf{x}) \quad (2)$$

where C_{ijkl} , e_{kij} , h_{ik} represent elastic, piezoelectric and dielectric material constants, respectively. $D_i(\mathbf{x})$ is the vector of the electric displacements; $\sigma_{ij}(\mathbf{x})$ is the stress tensor. The Cartesian coordinates are specified as $\mathbf{x} = (x_1, x_2, x_3)$. The strain tensor ε_{ij} and electric field vector E_k are related to the mechanical displacements u_i and electric potential ψ by

$$\varepsilon_{ij} = \frac{1}{2}(u_{i,j} + u_{j,i}), \quad E_k = -\psi_{,k} \quad (3)$$

The governing equations for a general piezoelectric body Ω under quasi-electrostatic and elastostatic assumptions are given by the equation of motion for the displacements and the first Maxwell's equation for the vector of electric displacements as

$$\sigma_{ij,j}(\mathbf{x}) + X_i(\mathbf{x}) = 0 \quad (4)$$

$$D_{i,i}(\mathbf{x}) + R(\mathbf{x}) = 0 \quad (5)$$

where $X_i(\mathbf{x})$ and $R(\mathbf{x})$ are the vector of the body forces and the volume density of the free electric charges, respectively.

The piezoelectric constitutive equations (1, 2), representing the coupling of mechanical and electric fields, may be written for a transversally isotropic 3-D piezoelectric body in a compact matrix form as

$$\begin{bmatrix} \sigma_{11} \\ \sigma_{22} \\ \sigma_{33} \\ \sigma_{23} \\ \sigma_{13} \\ \sigma_{12} \end{bmatrix} = \begin{bmatrix} c_{11} & c_{12} & c_{13} & 0 & 0 & 0 \\ c_{12} & c_{22} & c_{23} & 0 & 0 & 0 \\ c_{13} & c_{23} & c_{33} & 0 & 0 & 0 \\ 0 & 0 & 0 & c_{44} & 0 & 0 \\ 0 & 0 & 0 & 0 & c_{55} & 0 \\ 0 & 0 & 0 & 0 & 0 & c_{66} \end{bmatrix} \begin{bmatrix} \varepsilon_{11} \\ \varepsilon_{22} \\ \varepsilon_{33} \\ 2\varepsilon_{23} \\ 2\varepsilon_{13} \\ 2\varepsilon_{12} \end{bmatrix} - \begin{bmatrix} 0 & 0 & e_{31} \\ 0 & 0 & e_{31} \\ 0 & 0 & e_{33} \\ 0 & e_{15} & 0 \\ e_{15} & 0 & 0 \\ 0 & 0 & 0 \end{bmatrix} \begin{bmatrix} E_1 \\ E_2 \\ E_3 \end{bmatrix} \quad (6)$$

$$\begin{bmatrix} D_1 \\ D_2 \\ D_3 \end{bmatrix} = \begin{bmatrix} 0 & 0 & 0 & 0 & e_{15} & 0 \\ 0 & 0 & 0 & e_{15} & 0 & 0 \\ e_{31} & e_{31} & e_{33} & 0 & 0 & 0 \end{bmatrix} \begin{bmatrix} \varepsilon_{11} \\ \varepsilon_{22} \\ \varepsilon_{33} \\ 2\varepsilon_{23} \\ 2\varepsilon_{13} \\ 2\varepsilon_{12} \end{bmatrix} + \begin{bmatrix} h_{11} & 0 & 0 \\ 0 & h_{22} & 0 \\ 0 & 0 & h_{33} \end{bmatrix} \begin{bmatrix} E_1 \\ E_2 \\ E_3 \end{bmatrix} \quad (7)$$

At the global boundary Γ of the assumed 3-D body Ω , the essential boundary conditions for the displacements \tilde{u}_i and electric potentials $\tilde{\psi}$ as well as the natural boundary conditions for the surface tractions $\tilde{T}_i = \sigma_{ij}n_j$ and the surface density of the electric induction field flux (surface charge density) $\tilde{Q} = D_i n_i$ are defined with n_i being the unit normal vector.

3 LOCAL INTEGRAL EQUATIONS

The MLPG method is based on the local weak form of the governing equations (4, 5) that is written over the local subdomain Ω_s . The local subdomain is shown in Fig. 2. The local subdomain is a small region taken for each node inside the global domain (Atluri, 2004). The local subdomains could be of any geometrical shape; in this paper a spherical shape is used just for the sake of simplicity. The local weak forms can then be written as follows:

$$\int_{\Omega_s} \sigma_{ij,j}(\mathbf{x}, t) p^*(\mathbf{x}) d\Omega + \int_{\Omega_s} X_i(\mathbf{x}, t) p^*(\mathbf{x}) d\Omega = 0 \quad (8)$$

$$\int_{\Omega_s} D_{j,j}(\mathbf{x}, t) p^*(\mathbf{x}) d\Omega - \int_{\Omega_s} R(\mathbf{x}, t) p^*(\mathbf{x}) d\Omega = 0 \quad (9)$$

where $p^*(\mathbf{x})$ is a test function chosen as a Heaviside unit step function (Atluri, 2004; Sladek, *et al.*, 2012c).

The local integral equations (LIEs) are formed from the local weak forms (8, 9) with the use of the Gauss divergence theorem and the properties of the selected test function. Assuming both the body forces $X_i(\mathbf{x})$ and the volume density of free electric charges $R(\mathbf{x})$ to be vanishing in the present case, the LIEs take the following compact form:

$$\int_{\partial\Omega_s} \sigma_{ij}(\mathbf{x}) n_j(\mathbf{x}) d\Gamma = 0 \quad (10)$$

$$\int_{\partial\Omega_s} D_j(\mathbf{x}) n_j(\mathbf{x}) d\Gamma = 0 \quad (11)$$

where $n_j(\mathbf{x})$ is the unit outward normal vector to the boundary $\partial\Omega_s$ of the local subdomain.

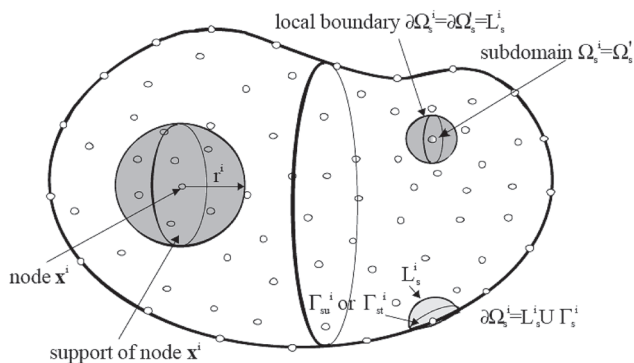


Fig. 2 Local boundaries and sub-domain for the weak formulation and support domain for the MLS approximation (Sladek *et al.*, 2009).

For the approximation of the trial functions, various approximation schemes such as radial basis functions (RBF), partition of unity (PU), reproducing kernel particle methods (RKPM) or moving least-squares (MLS) can be used (Atluri, 2004). In this paper, the MLS approximation is used for the approximation of the displacement and electric potential field in terms of the scattered nodal points as

$$u_j(\mathbf{x}) = \sum_{i=1}^n \phi^i(\mathbf{x}) \hat{u}_j^i, \quad \psi(\mathbf{x}) = \sum_{i=1}^n \phi^i(\mathbf{x}) \hat{\psi}^i \quad (12)$$

where the nodal values \hat{u}_j^i and $\hat{\psi}^i$ are so-called fictitious parameters for the mechanical displacements and electric potential, respectively. The MLS shape function $\phi^i(\mathbf{x})$ is defined over a set of n nodes located in the support domain Ω_s (Atluri, 2004). The C^1 -continuity of the MLS approximation is ensured by the fourth-order spline type weight function used for the construction of the shape function given as

$$v^a(\mathbf{x}) = \begin{cases} 1 - 6\left(\frac{d^a}{r^a}\right)^2 + 8\left(\frac{d^a}{r^a}\right)^3 - 3\left(\frac{d^a}{r^a}\right)^4 & 0 \leq d^a \leq r^a \\ 0 & d^a \geq r^a \end{cases} \quad (13)$$

where $d^a = \|\mathbf{x} - \mathbf{x}^a\|$ and r^a is the radius of the circular support domain. The value of n in eq. (12) is determined by the number of nodes lying in the support domain with radius r^a . The partial derivatives of the field quantities are approximated with the use of the shape function derivative $\phi_{,k}^i(\mathbf{x})$ and the same fictitious parameters as

$$u_{j,k}(\mathbf{x}) = \sum_{i=1}^n \phi_{,k}^i(\mathbf{x}) \hat{u}_j^i, \quad \psi_{,k}(\mathbf{x}, t) = \sum_{i=1}^n \phi_{,k}^i(\mathbf{x}) \hat{\psi}^i \quad (14)$$

Applying eqs. (12, 14) to the approximation of the trial functions $u_j(\mathbf{x})$, $\psi(\mathbf{x})$ and their derivatives in the constitutive relations (6, 7) and their subsequent insertion into the local integral equations (10, 11) leads to discretized local integral equations in the following form:

$$\sum_{i=1}^n \hat{u}_1^i \left(\int_{\partial\Omega_s} [n_1 c_{11} \phi_{,1}^i(\mathbf{x}) + n_2 c_{66} \phi_{,2}^i(\mathbf{x}) + n_3 c_{55} \phi_{,3}^i(\mathbf{x})] d\Gamma \right) + \sum_{i=1}^n \hat{u}_2^i \left(\int_{\partial\Omega_s} [n_1 c_{12} \phi_{,2}^i(\mathbf{x}) + n_2 c_{66} \phi_{,1}^i(\mathbf{x})] d\Gamma \right) + \sum_{i=1}^n \hat{u}_3^i \left(\int_{\partial\Omega_s} [n_1 c_{13} \phi_{,3}^i(\mathbf{x}) + n_3 c_{55} \phi_{,1}^i(\mathbf{x})] d\Gamma \right) + \sum_{i=1}^n \hat{\psi}^i \left(\int_{\partial\Omega_s} [n_1 e_{31} \phi_{,3}^i(\mathbf{x}) + n_3 e_{15} \phi_{,1}^i(\mathbf{x})] d\Gamma \right) = 0 \quad (15)$$

$$\sum_{i=1}^n \hat{u}_1^i \left(\int_{\partial\Omega_s} [n_1 c_{66} \phi_{,2}^i(\mathbf{x}) + n_2 c_{12} \phi_{,1}^i(\mathbf{x})] d\Gamma \right) + \sum_{i=1}^n \hat{u}_2^i \left(\int_{\partial\Omega_s} [n_1 c_{66} \phi_{,1}^i(\mathbf{x}) + n_2 c_{22} \phi_{,2}^i(\mathbf{x}) + n_3 c_{44} \phi_{,3}^i(\mathbf{x})] d\Gamma \right) + \sum_{i=1}^n \hat{u}_3^i \left(\int_{\partial\Omega_s} [n_2 c_{23} \phi_{,3}^i(\mathbf{x}) + n_3 c_{44} \phi_{,2}^i(\mathbf{x})] d\Gamma \right) + \sum_{i=1}^n \hat{\psi}^i \left(\int_{\partial\Omega_s} [n_2 e_{31} \phi_{,3}^i(\mathbf{x}) + n_3 e_{15} \phi_{,2}^i(\mathbf{x})] d\Gamma \right) = 0 \quad (16)$$

$$\begin{aligned} & \sum_{i=1}^n \hat{u}_1^i \left(\int_{\partial\Omega_3} [n_1 c_{55} \phi_{,3}^i(\mathbf{x}) + n_3 c_{13} \phi_{,1}^i(\mathbf{x})] d\Gamma \right) + \\ & + \sum_{i=1}^n \hat{u}_3^i \left(\int_{\partial\Omega_3} [n_1 c_{55} \phi_{,1}^i(\mathbf{x}) + n_2 c_{44} \phi_{,2}^i(\mathbf{x}) + n_3 c_{33} \phi_{,3}^i(\mathbf{x})] d\Gamma \right) + \\ & + \sum_{i=1}^n \hat{u}_2^i \left(\int_{\partial\Omega_3} [n_2 c_{44} \phi_{,3}^i(\mathbf{x}) + n_3 c_{23} \phi_{,2}^i(\mathbf{x})] d\Gamma \right) + \end{aligned} \quad (17)$$

$$+ \sum_{i=1}^n \hat{\psi}^i \left(\int_{\partial\Omega_3} [n_1 e_{15} \phi_{,1}^i(\mathbf{x}) + n_2 e_{15} \phi_{,2}^i(\mathbf{x}) + n_3 e_{33} \phi_{,3}^i(\mathbf{x})] d\Gamma \right) = 0$$

$$\begin{aligned} & \sum_{i=1}^n \hat{u}_1^i \left(\int_{\partial\Omega_3} [n_1 e_{15} \phi_{,3}^i(\mathbf{x}) + n_3 e_{31} \phi_{,1}^i(\mathbf{x})] d\Gamma \right) + \\ & + \sum_{i=1}^n \hat{u}_2^i \left(\int_{\partial\Omega_3} [n_2 e_{15} \phi_{,3}^i(\mathbf{x}) + n_3 e_{31} \phi_{,2}^i(\mathbf{x})] d\Gamma \right) + \\ & + \sum_{i=1}^n \hat{u}_3^i \left(\int_{\partial\Omega_3} [n_1 e_{15} \phi_{,1}^i(\mathbf{x}) + n_2 e_{15} \phi_{,2}^i(\mathbf{x}) + n_3 e_{33} \phi_{,3}^i(\mathbf{x})] d\Gamma \right) + \\ & + \sum_{i=1}^n \hat{\psi}^i \left(\int_{\partial\Omega_3} [n_1 h_{11} \phi_{,1}^i(\mathbf{x}) + n_2 h_{22} \phi_{,2}^i(\mathbf{x}) + n_3 h_{33} \phi_{,3}^i(\mathbf{x})] d\Gamma \right) = 0 \end{aligned} \quad (18)$$

A collocation approach is used to impose the essential boundary conditions directly, using the MLS variable approximations (12). For natural boundary conditions, local integral equations are written for the nodes on the appropriate segments of the global boundary as explained in (Atluri, 2004).

4 NUMERICAL EXAMPLES

The results of the numerical experiments are presented in this section to show the applicability of the proposed MLPG formulation for the analysis of a simplified piezoelectric sensor as the one shown in Fig. 1. A three-dimensional cylinder with a radius $r = 0,01$ m and height $h = 0,001$ m is considered. For convenience with the numerical examples presented, the centre of the bottom side of the cylinder is located 0.1 m in the x_1 direction away from the origin of the global coordinate system. The material of the cylinder is considered as a PZT-4 piezoelectric ceramic with the material constants given in (Stanak, et al., 2011). The geometry of the cylinder is discretized by using 804 nodal points. The radius of the MLS support domain is chosen as 0.006 m. The bottom of the assumed cylinder is clamped, which corresponds to the panel placed on a rigid support. The vanishing electric potential is prescribed at the bottom side, which corresponds to the grounding electrode attached there. The induced electric potential is measured at the top of the sensor.

As the first numerical example, a uniform mechanical displacement $\tilde{u}_3^{top} = -1 \times 10^{-8}$ is prescribed at the top of the cylinder. This corresponds to the loading applied to the panel directly above the sensor. The results obtained are compared to a FEM-Ansys solution that uses 900 higher-order piezoelectric elements for a quarter of the cylinder. The response of the induced electric potential to the uniform compressive load applied is shown in Fig. 3 for the nodes in a radial direction. Note that the response is symmetrical with respect to axis x_3 . Good agreement between the FEM and MLPG results is observed.

In the next example the non-uniform distribution of the mechanical displacement is considered. If the concentrated load applied to the composite panel is not acting straight above the sensor, but instead is shifted away, then the resulting displacement field will have a non-uniform distribution over the sensor. In the case considered here, the distribution of the displacement field over the nodal points on the top side of the cylindrical piezosensor is governed by the formula:

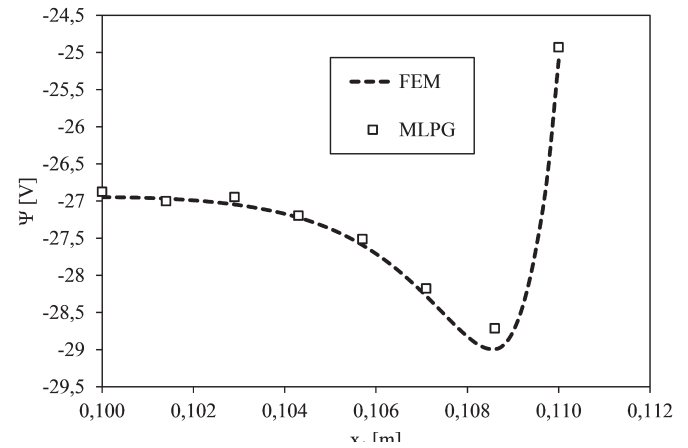


Fig. 3 Electric potential induced at the top of the piezosensor under a uniform load.

$$\tilde{u}_3^{top}(x_1, x_2, x_3 = h) = a + bx_1 + c(x_1)^2 \quad (19)$$

where a , b , c are arbitrary constants. For the compressive load the constants are taken as $a = -1,85 \times 10^{-8}$, $b = 1,3 \times 10^{-8}$ and $c = 9 \times 10^{-7}$. Figure 4 shows the schematic variation of the prescribed displacements over the sensor marked as a thick red line.

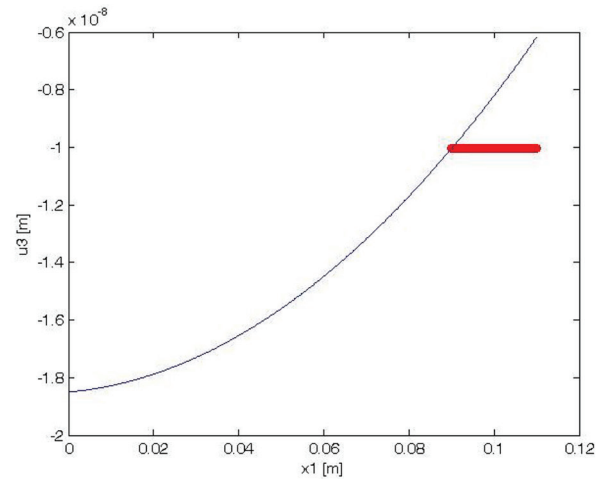


Fig. 4 Variation of the prescribed displacement field over the sensor (thick line).

The electrical response will no longer be symmetric in such a case of an applied load. Figure 5 presents the electric potential induced on the top side of the piezoelectric cylinder subjected to a non-uniform load. The deformed shape of the cylinder is presented in Fig. 6 via showing the shifting of the boundary nodes. Note that the resulting plot is magnified.

In certain cases a tensional displacement load may also occur with the opposite orientation of the vertical displacement applied. For such a case the constants in eq. (19) are chosen as $a = 1,61 \times 10^{-8}$, $b = 1,3 \times 10^{-8}$ and $c = -9 \times 10^{-7}$. The resulting displacement field at the top of the sensor is shown in Fig. 7 and the induced electric potential at the top of the sensor in Fig. 8.

The electric potential field induced is the primary quantity that is measured as an output of the piezoelectric sensor. The numerical results presented in Figures 5 and 8 indicate that a significant change in the electric potential is detected at the outer edge of the sensor. This is also obvious from Fig. 3 for the uniform load. Such an abrupt

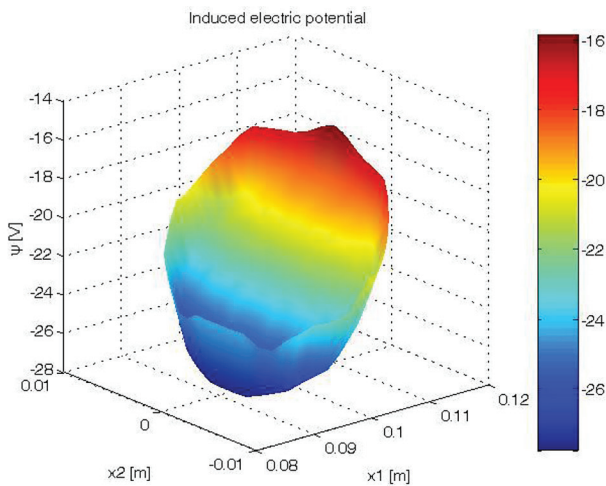


Fig. 5 Induced electric potential at the top of the sensor under a compressive load.

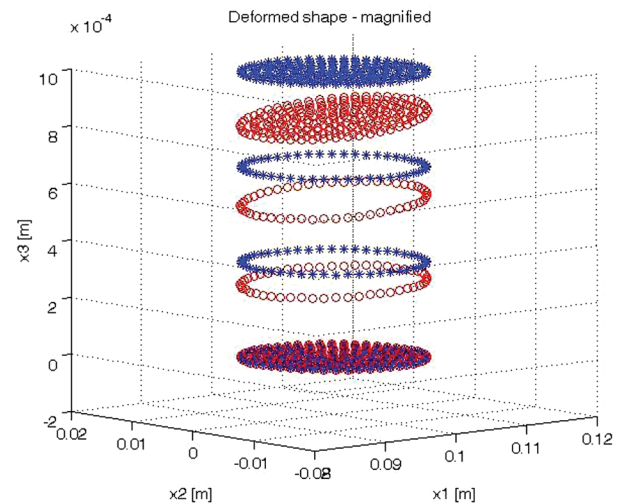


Fig. 6 Resulting deformed shape of the piezosensor under a compressive load (magnified 2×10^4 times).

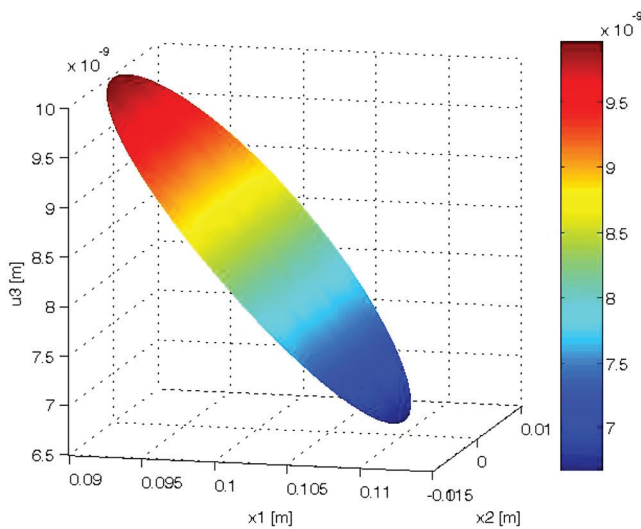


Fig. 7 Spatial variation of the vertical displacement field at the top of the sensor under a tensional load.

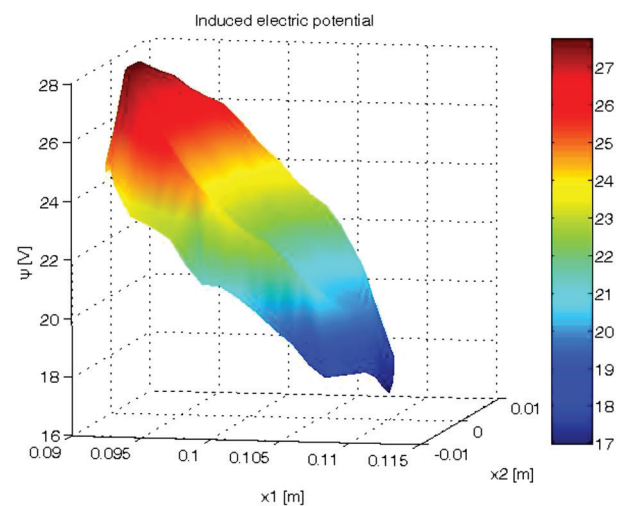


Fig. 8 Electric potential induced at the top of the sensor under a tensional load.

change may change the results of the measurement. The manufacturers of piezoelectric devices thus do not put the electrodes at the very edge of the sensor, but rather use smaller diameters as can also be observed in Fig. 1.

5 CONCLUSION

A meshless local Petrov-Galerkin method (MLPG) is proposed for the solution of boundary value problems for coupled electro-mechanical fields in piezoelectric solids. The proposed method is a truly meshless method as no discretization elements were used for the approximation or integration of any unknowns. The MLS approximation scheme has been used for the approximation of trial functions. Using the Heaviside unit step function as a test function, a pure boundary formulation on each local subdomain has been obtained.

The main advantage of the present method is its simplicity and generality in comparison to other techniques such as the conventional BEM. The method is particularly promising for problems which can-

not be solved by the conventional BEM in cases when the fundamental solutions are not available.

For the reliable functioning and design of piezoelectric devices, it is necessary to use advanced numerical methods. An electrical response to a mechanical load must be determined. The applicability of the proposed meshless method is demonstrated by the numerical examples assuming uniform and non-uniform mechanical displacement loading. The results indicate a significant change in the electric potential induced at the outer edge of the sensor. Thus the proper design of the electrodes can be envisaged. The meshless method presented may also be easily extended to the design of functionally graded piezoelectric devices.

Acknowledgement

The authors gratefully acknowledge the support by the Slovak Science and Technology Assistance Agency registered under No. APVV-0014-10.

REFERENCES

- Adachi, K. - Kitamura, Y. - Iwatsubo, T. (2004)** *Integrated design of piezoelectric damping system for flexible structure*. Applied Acoustics, 65, pp. 293-310.
- Agnes, G. S. (1995)** *Development of a modal model for simultaneous active and passive piezo-electric vibration suppression*. Journal of Intelligent Material Systems and Structures, 6, pp. 482-487.
- Ahmadian, M. - DeGiulio, A. P. (2001)** *Recent advances in the use of piezoceramics for vibration suppression*. The Shock and Vibration Digest, 33, 1, pp. 15-22.
- Atluri, S. N. (2004)** *The Meshless Method (MLPG) For Domain & BIE Discretizations*. Forsyth: Tech Science Press.
- Atluri, S. N. - Zhu, T. (1998)** *A new Meshless Local Petrov-Galerkin (MLPG) approach in computational mechanics*. Computational Mechanics, 22, pp. 117-127.
- Benjeddou, A. (2000)** *Advances in piezoelectric finite element modelling of adaptive structural elements: a survey*. Computers and Structures, 76, pp. 347-363.
- Ding H. - Liang J. (1999)** *The fundamental solutions for transversally isotropic piezoelectricity and boundary element method*. Computers & Structures, 71, pp. 447-455.
- Fur, L. S. - Yang, H. T. Y. - Ankireddi, S. (1996)** *Vibration control of tall buildings under seismic and wind loads*. ASCE Journal of Structural Engineering, 122, 8, pp. 948-957.
- Heyliger, P. (1997)** *Exact solutions for simply supported laminated piezoelectric plates*. Journal of Applied Mechanics, 64, pp. 299-306.
- Lancaster, P. - Salkauskas, T. (1981)** *Surfaces generated by moving-least square methods*. Mathematics in Computation, 37, pp. 141-158.
- Lee, J. S. (1995)** *Boundary element method for electroelastic interaction in piezoceramics*. Engineering Analysis with Boundary Elements, 15, pp. 321-328.
- Lerch, R. (1990)** *Simulation of piezoelectric devices by two- and three-dimensional finite elements*. IEEE Transactions on Ultrasonic and Ferroelectric Frequency Control, 37, pp. 233-247.
- Ray, M. C. - Bhattacharya, R. - Samanta, B. (1998)** *Exact solutions for dynamic analysis of composite plates with distributed piezoelectric layers*. Computers and Structures, 66, pp. 737-743.
- Sladek, J. - Sladek, V. - Krahulec, S. - Wunsche, M. - Zhang, Ch. (2012a)** *MLPG Analysis of Layered Composites with Piezoelectric and Piezomagnetic Phases*. CMC: Computers, Materials & Continua, 29, 1, pp. 75-101.
- Sladek, J. - Sladek, V. - Solek, P. (2009)** *Elastic analysis in 3D anisotropic functionally graded solids by the MLPG*. CMES: Computer Modeling in Engineering & Sciences, 43, pp. 223-251.
- Sladek, J. - Sladek, V. - Solek, P. - Saez, A. (2008)** *Dynamic 3D axisymmetric problems in continuously nonhomogeneous piezoelectric solids*. International Journal of Solids and Structures, 45, pp. 4523-4542.
- Sladek, J. - Sladek, V. - Stanak, P. (2010a)** *Analysis of thermo-piezoelectricity problems by meshless method*. Acta Mechanica Slovaca, 14, 4, pp. 16-27.
- Sladek, J. - Sladek, V. - Stanak, P. - Pan, E. (2010b)** *The MLPG for bending of electroelastic plates*. CMES – Computer Modeling in Engineering and Sciences, 64, pp. 267-298.
- Sladek, J. - Sladek, V. - Stanak, P. - Wen, P. H. - Atluri, S. N. (2012b)** *Laminated elastic plates with piezoelectric sensors and actuators*. CMES – Computer Modeling in Engineering and Sciences, 85, pp. 543-572.
- Sladek, J. - Sladek, V. - Stanak, P. - Zhang, Ch. - Wunsche, M. (2012c)** *Analysis of the bending of circular piezoelectric plates with functionally graded material properties by a MLPG method*. Engineering Structures, 47, pp. 81-89.
- Sladek, J. - Sladek, V. - Zhang, Ch. - Garcia-Sanchez, F. - Wunsche, M. (2006)** *Meshless Local Petrov-Galerkin Method for Plane Piezoelectricity*. CMC: Computers, Materials & Continua, 4, 2, pp. 109-117.
- Sladek, J. - Sladek, V. - Zhang, Ch. - Solek, P. - Starek, L. (2007)** *Fracture analyses in continuously nonhomogeneous piezoelectric solids by the MLPG*. CMES – Computer Modeling in Engineering and Sciences, 19, pp. 247-262.
- Song, G. - Sethi, V. - Li, H. N. (2006)** *Vibration control of civil structures using piezoceramic smart materials: A review*. Engineering Structures, 28, pp. 1513-1524.
- Stanak, P. - Sladek, J. - Sladek, V. - Krahulec, S. (2011)** *Composite circular plate analyzed as a 3-D axisymmetric piezoelectric solid*. Building Research Journal, 59, 3-4, pp. 125-140.
- Tiersten, H. F. (1969)** *Linear piezoelectric plate vibrations*. New York: Plenum Press.